

# A comparison between theoretical and numerical ultimate failure domains for pile groups

Francesco Potini<sup>1</sup> and Riccardo Conti<sup>1</sup>[0000-0001-7255-4537]

<sup>1</sup> Università degli Studi Niccolò Cusano, Roma, Italia  
francesco.potini@unicusano.it

**Abstract.** Multiaxial strength envelopes have been recently proposed as a rational approach for the design of pile foundations subjected to inclined and eccentric loads, leading to more economical solutions with respect to standard methods applied in the design practice. Theoretical solutions based on the application of the Upper-Bound (UB) and Lower-Bound (LB) theorem of Limit Analysis have been proposed to derive the ultimate failure domain of pile groups. In this paper, theoretical predictions for a 4×1 pile group embedded in a homogeneous clayey soil deposit are validated against the results of numerical analyses carried out with the Finite Element code Abaqus. To take into account the non-linear behaviour of reinforced concrete piles, a damaged plasticity model was used for the concrete, while the reinforcing bars were modelled as equivalent elastoplastic shell elements. The soil was modelled as a standard elastic-perfectly plastic material with a Tresca failure criterion to represent the undrained soil behaviour in a total stress analysis.

**Keywords:** Pile Foundations, Ultimate Failure Domains, Finite Element Analyses

## 1 Introduction

The scientific literature on numerical and experimental modelling of pile foundations in failure conditions is relatively recent. Based on the results of 3D Finite Element (FE) analyses, Gerolymos and Papakyriakopoulos [1] proposed a macro-element model for the analysis of single piles and pile groups under horizontal loads. Psychari and Anastasopoulos [2] analysed the nonlinear response of pile groups in clay, subjected to multiaxial loads. The Authors implemented a 3D FE model in Abaqus [6], using an elasto-plastic constitutive model with kinematic hardening for the soil and the Concrete Damage Plasticity model to describe the mechanical response of reinforced concrete (RC) piles. The same FE model was used by Sakellariadis and Anastasopoulos [3] to reproduce the experimental behaviour of a 2×1 pile group in a homogeneous deposit of saturated sand, as observed in small-scale centrifuge models. Centrifuge tests on reduced-scale models were carried out also by de Sanctis *et al.* [4], who analysed the

behaviour of a circular pile group embedded in kaolin clay, subjected to a vertical eccentric load.

As shown theoretically by Di Laora *et al.* [5] and numerically by Sakellariadis and Anastasopoulos [3], the moment capacity of a pile group subjected to a vertical eccentric load is a result of two concurrent resistance mechanisms. The first one,  $M_{ax}$ , is due to the axial loads acting into the piles of the group, while the second one,  $M_b$ , stems from the possible contribution given by the formation of plastic hinges at the piles' head. The latter mechanism can be relevant in the case of large-diameter piles.

Di Laora *et al.* [5] proposed an Upper-Bound (UB) solution for the ultimate failure domain of pile groups under vertical eccentric loads, based on two main assumptions, *i.e.*: (i) the piles exhibit a rigid-perfectly plastic behaviour and (ii) the connecting raft is a rigid body not in contact with the soil. The theoretical solution takes into consideration two possible connections between the piles and the cap: either a hinge-connection, thus including only the  $M_{ax}$  contribution to the moment capacity of the group, or a rigid-plastic internal fixity, thus taking into account both the  $M_{ax}$  and  $M_b$  contributions.

This work presents some of the results of 3D FE analyses carried out with the software Abaqus [6]. The main objective of the numerical study is to validate the theoretical solution proposed by Di Laora *et al.* [5].

## 2 Problem definition and numerical FE model

The case of a  $4 \times 1$  pile group was analysed. The RC piles have a diameter  $d = 1.5$  m, length  $L = 20$  m, and spacing  $s = 3d$ . A class C25/30 concrete is assumed for the RC piles, with a typical reinforcement ratio  $\rho = 1.8\%$  of B450C steel bars. The piles are embedded in a homogenous clay deposit with undrained shear strength  $s_u = 50$  kPa and unit weight  $\gamma = 20$  kN/m<sup>3</sup>. The initial geostatic stress state is characterised by a ratio  $\sigma_{h0}/\sigma_{v0} = 0.8$  between the total horizontal and vertical soil stress.

Total stress analyses were carried out, assuming undrained conditions. 8 node linear brick elements with reduced integration (C3D8R) were used both for the soil and the concrete. Reinforcement bars were modelled as an equivalent steel tube embedded in the concrete continuum elements, using 4 node linear surface elements with reduced integration (S4R).

Fig. 1 shows the FE mesh adopted in the analyses, where the size of the elements (piles and soil close to the foundation) was chosen based on a preliminary parametric study in order not to affect the numerical results. To maximize the computational efficiency, symmetrical conditions along the ( $y$ - $z$ ) plane passing through the piles' axis were considered. Standard constraints were applied to the model boundaries, *i.e.*: normal displacements were restrained along the vertical boundaries, while all displacements were fixed at the base. In order to reduce boundary effects, vertical boundaries were placed at a distance of  $10d$  from the piles' edge, while the base of the model was placed at a distance of  $5d$  from the pile's end.

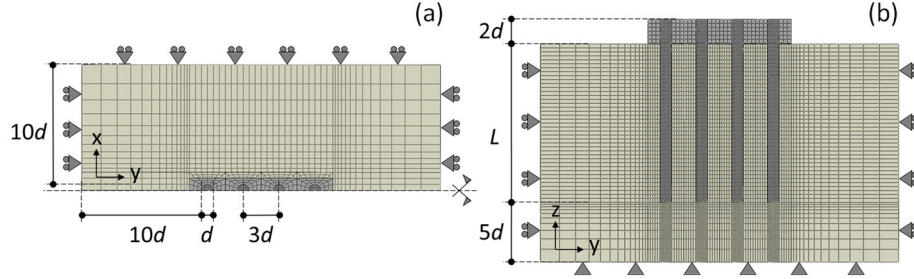


**Fig. 1.** Plane views of the mesh adopted for the 3D FE model of the 4x1 pile group: (a) horizontal x-y plane; (b) vertical y-z plane.

## 2.1 Constitutive models

A standard elastic-perfectly plastic constitutive model with a Tresca failure criterion and an associated flow rule was adopted for the soil. Table 1 summarizes the physical and constitutive parameters used in the analyses: the unit weight,  $\gamma$ ; the Young modulus,  $E = E_u$ ; the Poisson's ratio,  $\nu = \nu_u$ ; the friction angle,  $\phi = \phi_u$ ; the cohesion,  $c = s_u$  and the angle of dilatancy,  $\psi$ .

**Table 1.** Physical properties and constitutive parameters adopted for the soil

$\gamma$ [kN/m <sup>3</sup> ]	$E$ [MPa]	$\nu$	$\phi$ [°]	$c$ [kPa]	$\psi$ [°]
20	21.6	0.475	0	50	0

The concrete was modelled using the Concrete Damaged Plasticity (CDP) model implemented in Abaqus [6], which allows reproducing the highly nonlinear behaviour exhibited by the concrete under both monotonic compression and tension. Damage evolution laws were not taken into consideration in this work, as the latter define the typical response of concrete under cyclic loading.

Fig. 2 shows the stress-strain response assumed for the concrete under uniaxial conditions. The material behaviour in tension is linear until  $f_{t0}$ , beyond which a softening branch is detected. The stress-strain response in compression, instead, is linear-elastic until the yielding stress  $f_{c0}$ , beyond which a hardening and perfectly plastic behaviour is assumed until the failure stress  $f_{cu}$ . After  $f_{cu}$ , the material response follows a softening branch until complete failure due to crushing. Table 2 summarizes the physical and constitutive parameters adopted for the concrete: the dilation angle,  $\psi$ , and the eccentricity parameter,  $\epsilon$ , define the flow rule;  $K$  controls the shape of the yield surface;  $f_{b0}$  and  $f_{c0}$  are the concrete biaxial and uniaxial compressive strength, respectively;  $\mu^{visc}$  is a viscosity parameter, which allows regularizing the evolution laws of the material in the highly-nonlinear regime.

Finally, an isotropic elastic-perfectly plastic constitutive model was used for the reinforcement steel tube with a von Mises failure criterion and an associated flow rule.

The physical and constitutive parameters adopted in the analyses are:  $\gamma = 78 \text{ kN/m}^3$ ,  $E = 200 \text{ GPa}$ ,  $\nu = 0.2$  and yield strength  $f_y = 450 \text{ MPa}$ .

**Table 2.** Physical and constitutive parameters adopted for the CDP model.

$\gamma$ [kN/m <sup>3</sup> ]	$E$ [GPa]	$\nu$	$\psi$ [°]	$\varepsilon$	$f_{b0}/f_{c0}$	$K$	$\mu^{\text{visc}}$
20	21.5	0.15	30	0.1	1.16	0.667	$10^{-4}$

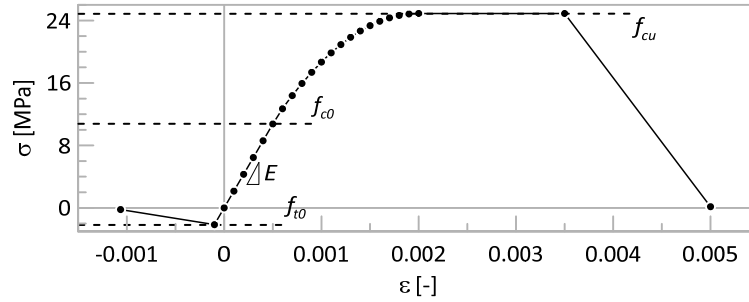


**Fig. 2.** Stress-strain response assumed for the concrete under uniaxial conditions.

## 2.2 Soil-pile interface

The pile-soil interface was modelled with tensionless contact elements, which allow both sliding and separation. An elastoplastic frictional behaviour was assumed for the interface, with the shear strength defined as:

$$\tau_{\text{lim}} = \mu \sigma_n (\leq \tau_{\text{max}}) \quad (1)$$

where  $\sigma_n$  is the normal stress acting on the interface,  $\mu$  is the friction coefficient and  $\tau_{\text{max}}$  is a threshold value for the maximum allowable shear strength. In order to obtain an equivalent cohesive behaviour of the interface along the whole pile length, a relatively high value of the friction coefficient was adopted ( $\mu = 2$ ), together with  $\tau_{\text{max}} = s_u$ .

## 3 FE model validation

### 3.1 Structural behaviour of the single pile

The simple case of a cantilever beam loaded by a concentrated load at the free edge was analysed to validate the structural behaviour of the RC piles. The beam has a circular transversal section ( $d = 1.5 \text{ m}$ ,  $\rho = 1.8\%$ ) and a length  $L = 15 \text{ m}$ . An axial load,  $N$ , is initially applied at the free edge, followed by a transversal displacement,  $v$ . The displacement is gradually increased until a plastic hinge forms at the fixed end of the beam.

Fig. 3(a) compares the numerical and theoretical moment-displacement curves for three values of  $N$ . The dependency of the moment capacity of the RC section on the applied axial load is well reproduced by the CDP model, except for the ultimate failure

condition, where, due to the confinement imposed by the steel tube, the numerical model exhibits a higher ductility compared with the theoretical one. As a result, the values of the bending moment at failure are slightly higher than theoretical predictions, as shown in Fig. 3(b).

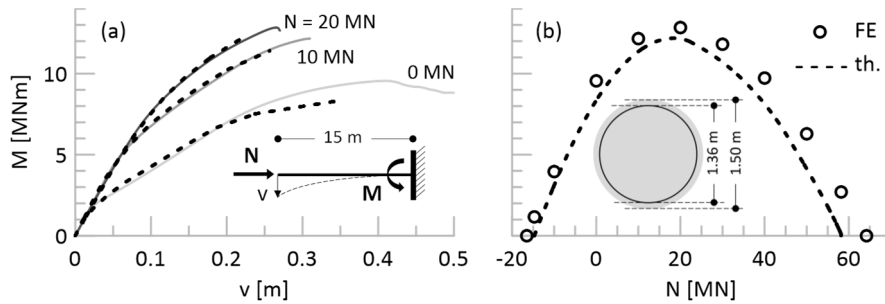


**Fig. 3.** Cantilever beam loaded by a concentrated load at the free edge. Comparison between numerical and theoretical results in terms of: (a)  $M$ - $v$  curves and (b)  $N$ - $M$  interaction diagram.

### 3.2 Vertical bearing capacity of the single pile

With the aim of validating the soil-pile numerical model, the case of a single pile subjected to a pure axial compression and uplift was modelled. The load is applied by imposing a vertical displacement at the pile head, and the results are compared with the theoretical predictions for the undrained bearing capacity under compression ( $N_u = 5.51$  MN) and uplift ( $S_u = 5.42$  MN).

Fig. 4 represents the load-displacement response of the single pile. The shaft resistance is fully mobilized for a relatively small displacement (about 20 mm), consistently with [7]. In compression, the pile-soil interface exhibits the expected cohesive behaviour. During uplift, instead, a gap between the pile and the surrounding soil forms close to the pile head, and the theoretical value of the shaft resistance is not reached. As expected, the base resistance is mobilized only at large pile displacements, and the numerical plateau of the corresponding load-displacement curve is in good agreement with the theoretical prediction.

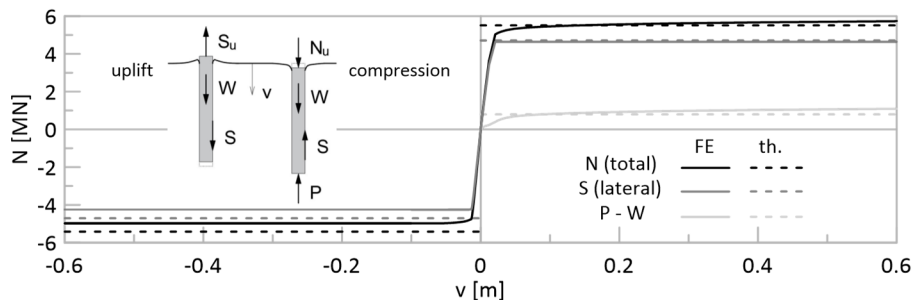


**Fig. 4.** Single pile subjected to a pure axial load in compression and uplift: comparison between numerical results and theoretical predictions.

#### 4 Analysis of the $4 \times 1$ pile group

In order to focus on the response of the sole pile group, the connecting raft is assumed not in contact with the soil in the 3D FE model.

The response of the pile group under pure axial compression and uplift is firstly investigated and compared with the single pile behaviour. As illustrated in Fig. 5, internal (2-3) and external (1-4) piles exhibit a slightly different response during the initial phase of the load-displacement path. When the shaft resistance is fully mobilized, all piles behave in the same fashion, showing a lower bearing capacity compared with the response of the single pile, due to interaction effects.

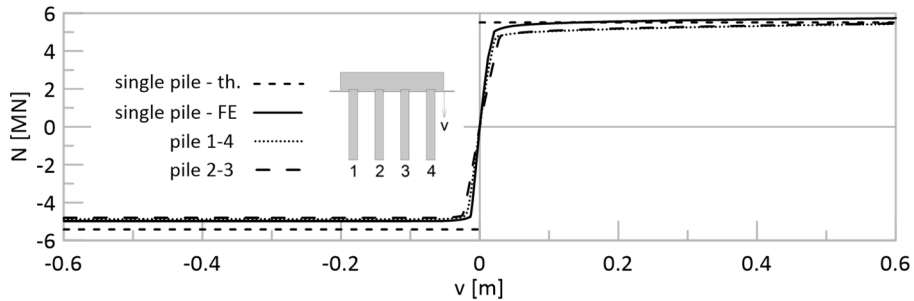


**Fig. 5.**  $4 \times 1$  pile group: comparison between the single pile and the pile group load-displacement response under pure axial compression and uplift.

The effect of a vertical eccentric load is simulated by imposing a rigid roto-translation to the connecting raft. In order to study the effects of the two resistance mechanisms,  $M_{ax}$  and  $M_b$ , both hinged and fixed connections are modelled between the pile cap and the raft.

Fig. 6 compares numerical and theoretical results for the ultimate ( $V$ ,  $M$ ) domain of the pile group. For the sake of consistency, the theoretical domain is computed using the numerical values of the bearing capacity of the single pile (Fig. 4) and the numerical  $N$ - $M$  interaction domain for the pile's cross section (Fig. 3b). For each applied  $V$ , the distance between the two failure domains provides the theoretical contribution  $M_b$  due to the formation of plastic hinges at the pile head. Numerical and theoretical domains are in good agreement, in the case of both hinged and fixed connections. However, due to piles interaction effects, the numerical domain is smaller than the corresponding theoretical one.

For the sole case of fixed pile-cap connection, Fig. 7 shows the key results referring to the five vertexes of the numerical domain shown in Fig. 6 (points (a)-(e)). Specifically, Fig. 7 shows: the axial force computed at the top of each pile ( $N_i$ ), together with the resultant vertical force on the group,  $V$ ; the contribution of the two bending resistance mechanisms developed with the cap rotation,  $\theta$ . For the sake of comparison, Fig. 7 shows also the corresponding theoretical values for the single pile. In cases (a) and (e) all piles are in uplift and compression, respectively. As a result, once all piles reach the same axial load, the moment capacity of the group is due only to  $M_b$ . In cases

(b), (c) and (d) the  $M_{ax}$  contribution is fully mobilised for relatively low cap rotations ( $\theta \approx 0.005$  rad), and it remains constant with increasing the displacement. As observed by Psychari and Anastasopoulos [2], the  $M_b$  contribution offers on average 30% of the bending resistance of the pile group, and, in all the analysed cases, it requires significant cap rotation to be fully mobilised ( $\theta = 0.03\div 0.04$  rad).

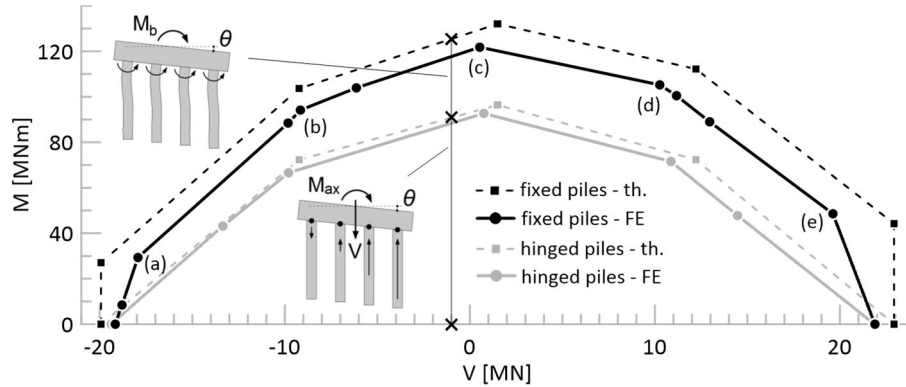
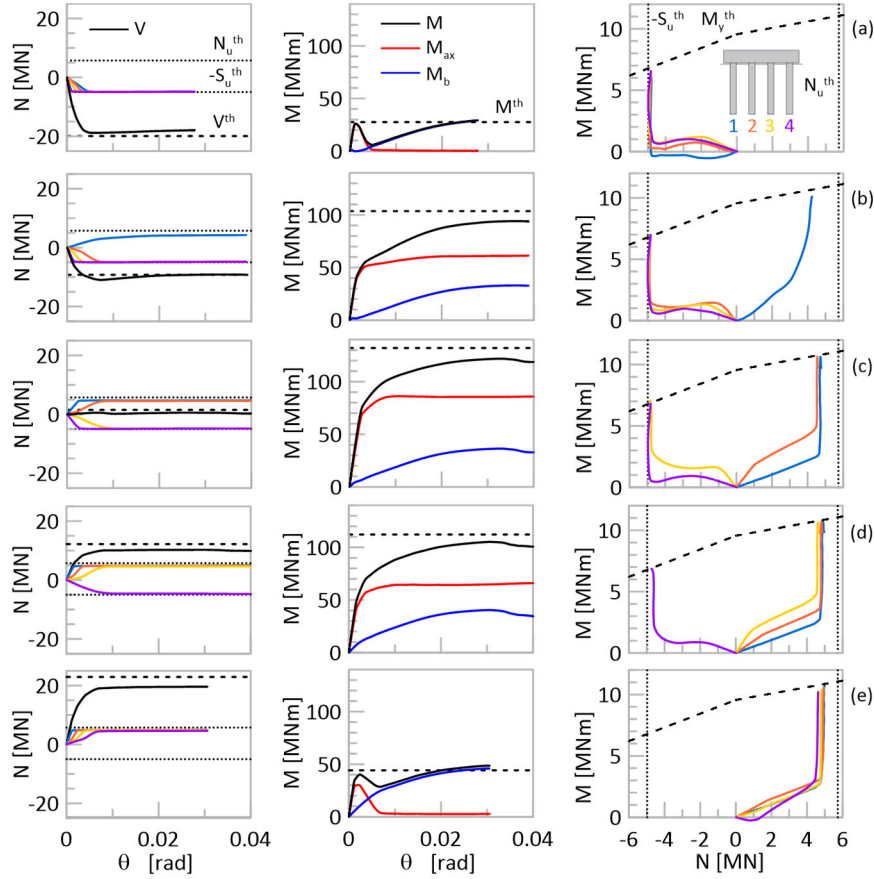


Fig. 6. 4×1 RC pile group ultimate failure domain: numerical-theoretical comparison.

## 5 Conclusions

In order to validate the vertical load-moment failure domain proposed by Di Laora *et al.* [5], a 3D FE model was implemented for a 4×1 RC pile group embedded in a clay deposit. The proposed numerical approach takes advantage of appropriate constitutive models for the soil, concrete and reinforcement, allowing to describe the nonlinear response of the foundation subjected to vertical eccentric loads. A preliminary study was conducted to assess the capability of the numerical model to reproduce the structural and geotechnical behaviour of the single pile. The Concrete Damaged Plasticity (CDP) model allows to take into account the  $N$ - $M$  interaction for RC piles under bending loads: plastic hinges develop and a realistic structural failure occurs. The pile-soil interaction is modelled using an interface that allows both sliding and gap under tension, calibrated to behave as an equivalent cohesive interface.

The numerical failure envelopes for the 4×1 pile group are in good agreement with the UB solution provided by Di Laora *et al.* [5], with minor differences essentially due to interaction effects between the piles, not included in the theoretical model. The two moment resistance mechanisms postulated by the theoretical model were observed in the numerical analyses. The moment capacity of the single piles plays a significant role in the overall strength of the pile group under vertical eccentric loads, particularly in the case of large-diameter piles. The numerical results showed the importance of considering also this latter mechanism, typically neglected in the design practice.



**Fig. 7.** 4×1 RC pile group FE results: axial load and bending moment capacity developed with cap rotation; piles head cross section  $N$ - $M$  interaction.

## References

1. Gerolymos, N., Papakyriakopoulos, O. (2016). Macroelement Modelling of Laterally Loaded Piles and Pile-groups.
2. Psychari, A., Anastasopoulos, I. (2022). Combined loading of RC pile groups in clay accounting for N–M interaction. *Soil Dynamics and Earthquake Engineering*, 163, 107490.
3. Sakellariadis, L., & Anastasopoulos, I. (2022). On the mechanisms governing the response of pile groups under combined VHM loading. *Géotechnique*, 1-22.
4. De Sanctis, L., Di Laora, R., Garala, T. K., Madabhushi, S. P. G., Viggiani, G. M. B., & Fagnoli, P. (2021). Centrifuge modelling of the behaviour of pile groups under vertical eccentric load. *Soils and Foundations*, 61(2), pp. 465-479.
5. Di Laora, R., de Sanctis, L., Aversa, S. (2019). Bearing capacity of pile groups under vertical eccentric load. *Acta Geotech* 14(1), pp. 193-205.
6. ABAQUS, Inc.. ABAQUS 2019 User's Manual. Dassault Systèmes Simulia Corp (2019).
7. Viggiani, C. (1999). *Fondazioni*. Helvelius Edizioni.